# Substituent Effects in the Binding of Alkali Metal Ions to Pyridines Studied by Threshold Collision-Induced Dissociation and ab Initio Theory: The Aminopyridines

**M. T. Rodgers**

*Department of Chemistry, Wayne State University, Detroit, Michigan 48202*

*Received: April 24, 2001; In Final Form: June 27, 2001*

Threshold collision-induced dissociation of $M^+$(*x*-aminopyridine) with xenon is studied using guided ion beam mass spectrometry. $M^+$ include the following alkali metal ions: $Li^+$, $Na^+$, and $K^+$. All three structural isomers are examined, $x$ = ortho, meta, and para. In all cases, the primary product corresponds to endothermic loss of the intact *x*-aminopyridine molecule, with minor production of $MXe^+$ formed by ligand exchange. The cross section thresholds are interpreted to yield zero and 298 K bond dissociation energies for $M^+$−*x*-aminopyridine after accounting for the effects of multiple ion-molecule collisions, internal energy of the reactant ions, and dissociation lifetimes. Ab initio calculations at the MP2(full)/6-31G* level of theory are used to determine the structures of these complexes and provide molecular constants necessary for the thermodynamic analysis of the experimental data. Theoretical bond dissociation energies are determined from single point calculations at the MP2(full)/6-311+G(2d,2p) level using the MP2(full)/6-31G* optimized geometries. Excellent agreement between theory and experiment is found for the $Na^+$ and $K^+$ systems, whereas the theoretical bond dissociation energies to $Li^+$ systems are systematically low but still within experimental error. The measured bond energies are compared among the systems examined here, and to the analogous methyl-substituted systems examined in a previous study, to determine the influence of the position and the nature of the substituent on the binding and factors that control the strength of such binding.

## Introduction

In recent work, we have developed methods to allow the application of quantitative threshold collision-induced dissociation methods to obtain accurate thermodynamic information on increasingly large systems.[1−12] One of the driving forces behind these developments is our interest in applying such techniques to large systems such as those of biological relevance. In addition, we seek to perform accurate thermochemical measurements that provide absolute anchors for metal cation affinity scales over an ever-broadening range of energies and molecular systems.

Among the systems examined in these earlier studies are a number of nitrogen-based heterocycles and several of the nucleic acid bases with alkali, alkaline earth and transition-metal ions.[5−12] These systems were chosen as models of nocovalent interactions with nucleic acids and a wide variety of nitrogen-based heterocycles of biological importance. We began these investigations with ligands possessing only a single functional group. This fundamental approach has allowed us to examine systematically the influence of the electronic structure of the metal ion and the polarizability, dipole moment, and tautomeric form of the ligand, as well as the effects that chelation and steric interactions have upon the strength of binding in these systems. Because the nucleic acid bases, modified bases, and other biologically relevant systems possess amino, hydroxy, and methyl substituents, we have recently initiated studies to extend this work by examining substituted pyridine systems.[11] These theoretical and experimental studies examine the intrinsic effects of varying the chemical identity of both the metal ion ($Li^+$, $Na^+$, and $K^+$) and the substituent ($CH_3$, $NH_2$, and OH), as well as the position of the substituent relative to the pyridyl nitrogen atom-binding site (ortho, meta, and para).

In the present study, we use guided ion beam mass spectrometry to collisionally excite complexes of $M^+$ bound to the structural isomers (ortho, meta, and para) of *x*-aminopyridine (*x*-$NH_2$Pyr), where $M^+ = Li^+$, $Na^+$, and $K^+$. The structures of the *x*-$NH_2$Pyr isomers are shown in Figure 1 along with their calculated dipole moments (determined here) and estimated polarizabilities.[13] The kinetic energy-dependent cross sections for the collision-induced dissociation (CID) processes are analyzed using methods developed previously.[3] The analysis explicitly includes the effects of the internal and translational energy distributions of the reactants, multiple collisions, and the lifetime for dissociation. We derive $M^+$−*x*-$NH_2$Pyr bond dissociation energies (BDEs) for all of the complexes and compare these results to ab initio calculations performed here. Comparison is also made to the analogous methyl-substituted pyridines to examine influence of these substituents on the binding and factors that control the strength of such binding.

## Experimental Section

**General Procedures.** Cross sections for CID of $M^+$(*x*-$NH_2$-Pyr), where $x$ = ortho, meta, and para, and $M^+ = Li^+$, $Na^+$, and $K^+$, are measured using a guided ion beam mass spectrometer that has been described in detail previously.[11] The $M^+$(*x*-$NH_2$Pyr) complexes are generated as described below. The ions are extracted from the source, accelerated, and focused into a magnetic sector momentum analyzer for mass analysis. Mass-selected ions are decelerated to a desired kinetic energy and focused into an octopole ion guide, which traps the ions in the radial direction.[14] The octopole passes through a static gas cell containing xenon, used as the collision gas, for reasons described elsewhere.[15−17] Low gas pressures in the cell (typically 0.05−

10.1021/jp011555z CCC: $20.00 
Published on Web 08/14/2001

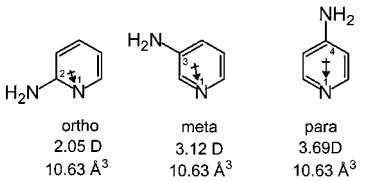


**Figure 1.** Structure of the *x*-aminopyridine molecules. Properly scaled dipole moments in Debye are shown for each as an arrow. Values for the dipole moment are determined from theoretical calculations performed here. The estimated polarizability is also shown.[13]

0.20 mTorr) are used to ensure that multiple ion-molecule collisions are improbable. Product and unreacted beam ions drift to the end of the octopole where they are focused into a quadrupole mass filter for mass analysis and subsequently detected with a secondary electron scintillation detector and standard pulse counting techniques.

Ion intensities are converted to absolute cross sections as described previously.[18] Absolute uncertainties in cross section magnitudes are estimated to be ±20%, which are largely the result of errors in the pressure measurement and the length of the interaction region. Relative uncertainties are approximately ±5%. Because the radio frequency used for the octopole does not trap light masses with high efficiency, the cross sections for $Li^+$ products were more scattered and showed more variations in magnitude than is typical for heavier ions. Therefore, absolute magnitudes of the cross sections for production of $Li^+$ are probably accurate to ±50%.

Ion kinetic energies in the laboratory frame, $E_{lab}$, are converted to energies in the center of mass frame, $E_{CM}$, using the formula $E_{CM} = E_{lab}\, m/(m + M)$, where $M$ and $m$ are the masses of the ionic and neutral reactants, respectively. All energies reported below are in the CM frame unless otherwise noted. The absolute zero and distribution of the ion kinetic energies are determined using the octopole ion guide as a retarding potential analyzer as previously described.[18] The distribution of ion kinetic energies is nearly Gaussian with a fwhm typically between 0.2 and 0.4 eV (lab) for these experiments. The uncertainty in the absolute energy scale is ± 0.05 eV (lab).

Even when the pressure of the reactant neutral is low, it has previously been demonstrated that the effects of multiple collisions can significantly influence the shape of CID cross sections.[19] Because the presence and magnitude of these pressure effects is difficult to predict, we have performed pressure-dependent studies of all cross sections examined here. In the present systems, we observe small cross sections at low energies that have an obvious dependence upon pressure. We attribute this to multiple energizing collisions that lead to an enhanced probability of dissociation below threshold as a result of the longer residence time of these slower moving ions. Data free from pressure effects are obtained by extrapolating to zero reactant pressure, as described previously.[19] Thus, results reported below are due to single bimolecular encounters.

**Ion Source.** The $M^+$(*x*-$NH_2$Pyr) complexes are formed in a 1-m long flow tube[11] operating at a pressure of 0.7−1.1 Torr with a helium flow rate of 4000−7000 sccm. Metal ions are generated in a continuous dc discharge by argon ion sputtering of a cathode, made from tantalum or iron, with a cavity containing the alkali metal. Typical operating conditions of the discharge for alkali metal ion production are 2−3.5 kV and 20−30 mA in a flow of roughly 10% argon in helium. The $M^+$(*x*-$NH_2$Pyr) complexes are formed by associative reactions of the alkali metal ion with the neutral *x*-$NH_2$Pyr, which is introduced into the flow 20−50 cm downstream from the dc discharge. Although the vapor pressure of all of the *x*-$NH_2$Pyr ligands was sufficient to carry out these experiments, increased ion signals were obtained by flowing helium over the sample. The flow conditions used in this ion source provide in excess of $10^5$ collisions between an ion and the buffer gas, which should thermalize the ions both vibrationally and rotationally. In our analysis of the data, we assume that the ions produced in this source are in their ground electronic states and that the internal energy of the $M^+$(*x*-$NH_2$Pyr) complexes is well described by a Maxwell−Boltzmann distribution of ro-vibrational states at 300 K. Previous work from this[8−12] and the Armentrout laboratories has shown that these assumptions are generally valid.[15,19−23]

**Thermochemical Analysis.** The threshold regions of the reaction cross sections are modeled using eq 1,

$$\sigma(E) = \sigma_0 \sum_i g_i (E + E_i - E_0)^n / E \qquad (1)$$

where $\sigma_0$ is an energy independent scaling factor, $E$ is the relative translational energy of the reactants, $E_0$ is the threshold for reaction of the ground electronic and ro-vibrational state, and $n$ is an adjustable parameter. The summation is over the ro-vibrational states of the reactant ions, $i$, where $E_i$ is the excitation energy of each state and $g_i$ is the population of those states ($\Sigma g_i = 1$). The populations of excited ro-vibrational levels are not negligible even at 298 K as a result of the many low-frequency modes present in these ions. The relative reactivity of all ro-vibrational states, as reflected by $\sigma_0$ and $n$, is assumed to be equivalent.

To obtain model structures, vibrational frequencies, and energetics for the neutral and metalated *x*-$NH_2$Pyr, ab initio calculations were performed using Gaussian 98.[24] Geometry optimizations were performed at the MP2(full)/6-31G* level. Vibrational analyses of the geometry-optimized structures were performed to determine the vibrational frequencies of the reactant ions and product molecules. When used to model the data or to calculate thermal energy corrections, the MP2(full)/6-31G* vibrational frequencies are scaled by a factor of 0.9646.[25] The scaled vibrational frequencies thus obtained for the nine systems studied are available as supplementary information and are listed in Table S1, whereas Table S2 lists the rotational constants.

The Beyer−Swinehart algorithm[26] is used to evaluate the density of the ro-vibrational states and the relative populations, $g_i$, are calculated by an appropriate Maxwell−Boltzmann distribution at the 298 K temperature appropriate for the reactants. The average vibrational energy at 298 K of the metal ion-bound *x*-$NH_2$Pyr is also given in Table S1. We have estimated the sensitivity of our analysis to the deviations from the true frequencies by scaling the calculated frequencies to encompass the range of average scaling factors needed to bring calculated frequencies into agreement with experimentally determined frequencies found by Pople et al.[27] Thus, the originally calculated vibrational frequencies were increased and decreased by 10%. The corresponding change in the average vibrational energy is taken to be an estimate of one standard deviation of the uncertainty in vibrational energy (Table S1) and is included in the uncertainties, also reported as one standard deviation, listed with the $E_0$ values.

We also consider the possibility that collisionally activated complex ions do not dissociate on the time scale of our experiment (about $10^{-4}$ s, but obviously energy dependent) by including statistical theories for unimolecular dissociation, specifically Rice−Ramsperger−Kassel−Marcus (RRKM) theory, into eq 1 as described in detail elsewhere.[3,22] This requires sets

of ro-vibrational frequencies appropriate for the energized molecules and the transition states (TSs) leading to dissociation. The former sets are given in Tables S1 and S2, whereas we assume that the TSs are loose and product-like because the interaction between the metal ion and the *x*-$NH_2$Pyr ligand is largely electrostatic. In this case, the TS vibrations used are the frequencies corresponding to the products, which are also found in Table S1. The transitional frequencies, those that become rotations of the completely dissociated products, are treated as rotors, a treatment that corresponds to a phase space limit (PSL) and is described in detail elsewhere.[3] For the $M^+$(*x*-$NH_2$Pyr) complexes, the two transitional mode rotors have rotational constants equal to those of the neutral *x*-$NH_2$Pyr product with axes perpendicular to the reaction coordinate. These are listed in Table S2. The external rotations of the energized molecule and TS are also included in the modeling of the CID data. The external rotational constants of the TS are determined by assuming that the TS occurs at the centrifugal barrier for interaction of $M^+$ with the neutral *x*-$NH_2$Pyr ligand, calculated variationally as outlined elsewhere.[3] The 2-D external rotations are treated adiabatically but with centrifugal effects included, consistent with the discussion of Waage and Rabinovitch.[28] In the present work, the adiabatic 2-D rotational energy is treated using a statistical distribution with explicit summation over the possible values of the rotational quantum number, as described in detail elsewhere.[3]

The model represented by eq 1 is expected to be appropriate for translationally driven reactions[29] and has been found to reproduce reaction cross sections well in a number of previous studies of both atom−diatom and polyatomic reactions,[30,31] including CID processes.[1,2,15,19,21,22,32−34] The model is convoluted with the kinetic energy distributions of both reactants, and a nonlinear least-squares analysis of the data is performed to give optimized values for the parameters $\sigma_0$, $E_0$, and $n$. The error associated with the measurement of $E_0$ is estimated from the range of threshold values determined for different zero-pressure extrapolated data sets, variations associated with uncertainties in the vibrational frequencies, and the error in the absolute energy scale, 0.05 eV (lab). For analyses that include the RRKM lifetime effect, the uncertainties in the reported $E_0$ values also include the effects of increasing and decreasing the time assumed available for dissociation (or equivalently, the distance traveled between the collision and detection) by a factor of 2.

Equation 1 explicitly includes the internal energy of the ion, $E_i$. All energy available is treated statistically, which should be a reasonable assumption because the internal (rotational and vibrational) energy of the reactants is redistributed throughout the ion upon impact with the collision gas. The threshold for dissociation is by definition the minimum energy required leading to dissociation and thus corresponds to formation of products with no internal excitation. The assumption that products formed at threshold have an internal temperature of 0 K has been tested for several systems.[1,2,15,16,21,22] It has also been shown that treating all energy of the ion (vibrational, rotational, and translational) as capable of coupling into the dissociation coordinate leads to reasonable thermochemistry. The threshold energies for dissociation reactions determined by analysis with eq 1 are converted to 0 K bond energies by assuming that $E_0$ represents the energy difference between reactants and products at 0 K.[35] This assumption requires that there are no activation barriers in excess of the endothermicity of dissociation. This is generally true for ion−molecule reactions[30] and should be valid for the simple heterolytic bond fission reactions examined here.[36]

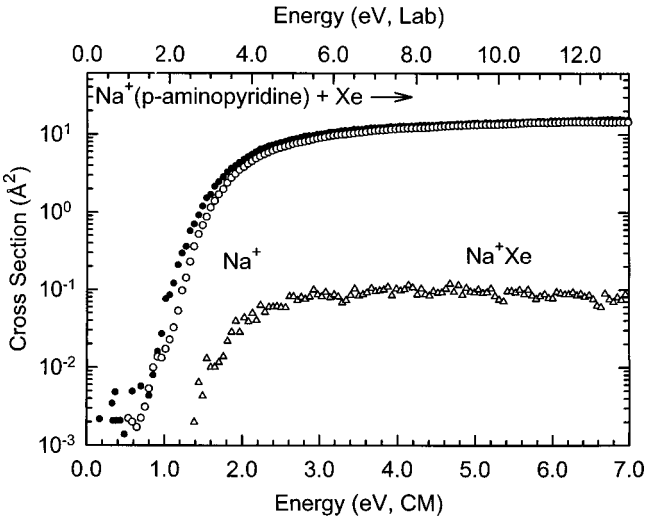


**Figure 2.** Cross sections for the collision-induced dissociation of the $Na^+$(*p*-aminopyridine) complex with Xe as a function of the kinetic energy in the center-of-mass frame (lower *x*-axis) and laboratory frame (upper *x*-axis). Data for the $Na^+$ product channel are shown for a Xe pressure of ∼0.2 mTorr (●) and extrapolated to zero (○). The cross section for the ligand exchange process to form $M^+Xe$ is also shown (△).

## Results

**Cross Sections for Collision-Induced Dissociation.** Experimental cross sections were obtained for the interaction of Xe with nine $M^+$(*x*-$NH_2$Pyr) complexes, where $M^+ = Li^+$, $Na^+$, and $K^+$ and $x$ = ortho, meta, and para. Figure 2 shows representative data for the $Na^+$(*p*-$NH_2$Pyr) complex. A complete set of figures for all nine $M^+$(*x*-aminopyridine) complexes are available in the Supporting Information as Figure S1. As discussed above, the dependence of the cross sections on pressure observed in the $M^+$ product data at the lowest energies, Figure 2, are a consequence of multiple collisions. A true single collision cross section for CID is obtained when the data are extrapolated to zero pressure of the Xe reactant as shown in Figure 2. The other $M^+$(*x*-$NH_2$Pyr) complexes show similar relative behavior. The most favorable process for all complexes is the loss of the intact *x*-$NH_2$Pyr molecule in the CID reactions 2.

$$M^+(x\text{-}NH_2Pyr) + Xe \rightarrow M^+ + x\text{-}NH_2Pyr + Xe \quad (2)$$

The magnitudes of the cross sections increase in size from $M^+ = Li^+$ to $Na^+$ to $K^+$. This is largely because the thresholds decrease in this same order. The only other product that is observed in the interaction of the complexes with Xe is the result of a ligand exchange process to form $MXe^+$. The cross sections for the $MXe^+$ products are approximately 1−3 orders of magnitude smaller than those of the primary dissociation product, $M^+$, and the thresholds are slightly lower (by the $M^+$−Xe binding energy), which is difficult to discern on the logarithmic scale. As little systematic information can be gleaned from these products, they will not be discussed further. However, it is conceivable that this ligand exchange process might cause a competitive shift in the observed thresholds. Within the quoted experimental errors, we do not believe such competition is likely to affect our threshold measurements in any of these systems for several reasons that have been detailed elsewhere.[37]

**Threshold Analysis.** The model of eq 1 was used to analyze the thresholds for eq 2 in nine $M^+$(*x*-$NH_2$Pyr) systems. The results of these analyses are provided in Table 1 for all nine

**TABLE 1: Fitting Parameters of Eq 1, Threshold Dissociation Energies at 0 K, and Entropies of Activation at 1000 K of $M^+L$[a]**

| $M^+L$ | $\sigma 0$[b] | n[b] | $E_0$[c] (eV) | $E_0$(PSL) (eV) | kinetic shift (eV) | $\Delta S^\dagger$(PSL) (J mol$^{-1}$ K$^{-1}$) |
|---|---|---|---|---|---|---|
| $Li^+$(*o*-aminopyridine) | 3.4 (0.2) | 1.5 (0.1) | 2.91 (0.33) | 2.46 (0.22) | 0.45 | 42 (2) |
| $Na^+$(*o*-aminopyridine) | 20.5 (3.7) | 1.1 (0.1) | 1.63 (0.07) | 1.52 (0.06) | 0.11 | 30 (2) |
| $K^+$(*o*-aminopyridine) | 45.0 (4.4) | 1.1 (0.1) | 1.08 (0.04) | 1.07 (0.04) | 0.01 | 33 (2) |
| $Li^+$(*m*-aminopyridine) | 3.2 (0.4) | 1.6 (0.1) | 2.45 (0.13) | 2.09 (0.10) | 0.36 | 27 (2) |
| $Na^+$(*m*-aminopyridine) | 19.5 (0.6) | 1.1 (0.1) | 1.49 (0.05) | 1.41 (0.04) | 0.08 | 23 (2) |
| $K^+$(*m*-aminopyridine) | 36.5 (0.5) | 1.1 (0.1) | 1.06 (0.04) | 1.05 (0.03) | 0.01 | 16 (2) |
| $Li^+$(*p*-aminopyridine) | 5.0 (1.6) | 1.3 (0.2) | 2.86 (0.33) | 2.25 (0.21) | 0.61 | 10 (2) |
| $Na^+$(*p*-aminopyridine) | 17.8 (0.6) | 1.1 (0.1) | 1.65 (0.05) | 1.52 (0.05) | 0.13 | 19 (2) |
| $K^+$(*p*-aminopyridine) | 36.3 (0.8) | 1.0 (0.1) | 1.16 (0.04) | 1.13 (0.03) | 0.03 | 14 (2) |

[a] Uncertainties are listed in parentheses. [b] Average values for loose PSL transition state. [c] No RRKM analysis.

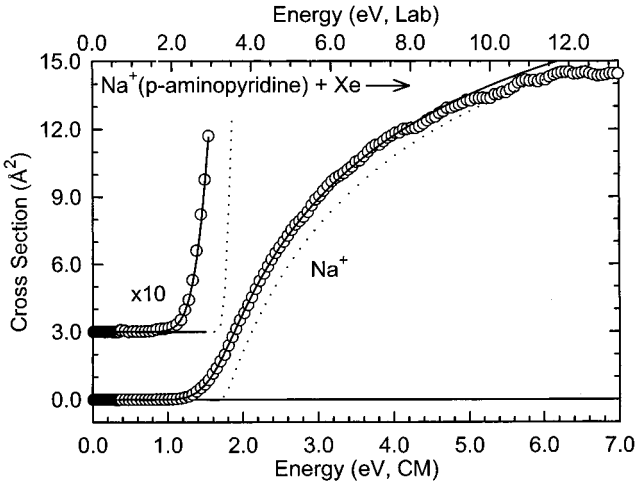


**Figure 3.** Zero-pressure-extrapolated cross section for collision-induced dissociation of the $Na^+$(*p*-aminopyridine) complex with Xe in the threshold region as a function of kinetic energy in the center-of-mass frame (lower *x*-axis) and the laboratory frame (upper *x*-axis). A solid line shows the best fit to the data using eq 1 convoluted over the neutral and ion kinetic energy distributions. A dashed line shows the model cross sections in the absence of experimental kinetic energy broadening for reactants with an internal energy corresponding to 0 K.

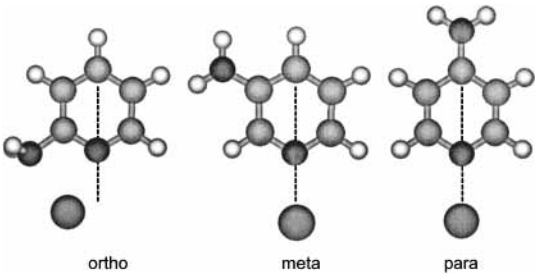


**Figure 4.** Optimized MP2(full)/6-31G* geometries of $Na^+$(*x*-aminopyridine), where *x* = ortho, meta, and para. All atoms lie in the plane of the molecule except for the amino hydrogen atoms in the ortho isomer complex.

complexes, and a representative analysis is shown in Figure 3 for the $Na^+$(*p*-$NH_2$Pyr) complex. A comparable set of figures for all nine $M^+$(*x*-aminopyridine) complexes are available in the Supporting Information as Figure S2. In all cases, the experimental cross sections for eq 2 are accurately reproduced using a loose PSL TS model.[3] Previous work has shown that this model provides the most accurate assessment of the kinetic shifts for CID processes for electrostatic ion−molecule complexes.[1−9,11,32,33] Good reproduction of the data is obtained over energy ranges exceeding 2.0 eV and cross section magnitudes of at least a factor of 100. Table 1 also includes values of $E_0$ obtained without including the RRKM lifetime analysis. Comparison of these values with the $E_0$(PSL) values shows that the kinetic shifts observed for these systems vary from 0.02 ± 0.01 eV for the $K^+$ systems, to 0.11 ± 0.03 eV for $Na^+$, and 0.47 ± 0.13 eV for $Li^+$. The total number of vibrations, 36, and heavy atoms, 8, remains the same in all nine $M^+$(*x*-$NH_2$Pyr) complexes, and hence the number of low-frequency vibrations remains the same. This implies that the observed kinetic shift should directly correlate with the density of states of the complex at threshold, which depends on the measured BDE. This is exactly what is found, as shown in Table 1.

The entropy of activation, $\Delta S^\dagger$, is a measure of the looseness of the TS and a reflection of the complexity of the system. It is largely determined by the molecular parameters used to model the energized molecule and the TS but also depends on the threshold energy. Listed in Table 1, $\Delta S^\dagger$ (PSL) values at 1000 K show modest variation, as expected on the basis of the similarity of these systems, and range between 10 and 42 J K$^{-1}$ mol$^{-1}$ across these systems. These entropies of activation can be favorably compared to a wide variety of noncovalently bound complexes previously measured in our laboratory,[1−12] and to the $\Delta S^\dagger_{1000}$ values in the range of 29−46 J K$^{-1}$ mol$^{-1}$ collected by Lifshitz for several simple bond cleavage dissociations of ions.[38]

**Theoretical Results.** Theoretical structures for neutral *x*-$NH_2$-Pyr ligands and for the complexes of these ligands with $H^+$, $Li^+$, $Na^+$, and $K^+$ were calculated as described above. Table S3 gives details of the final geometries for each of these species. Results for the most stable conformation of each $Na^+$(*x*-$NH_2$-Pyr) complex are shown in Figure 4.[39] The neutral molecules are very nearly planar with a slight distortion of the amino group out of the plane. Not surprisingly, the calculations find that the metal ions and proton prefer to be bound to the pyridyl nitrogen atom in the plane of the *x*-$NH_2$Pyr molecule rather than to the $\pi$-cloud of the aromatic ring. An exception to this is observed in the $K^+$(*o*-$NH_2$Pyr) complex as discussed below. In general, the distortion of the *x*-$NH_2$Pyr molecule that occurs upon complexation to a metal ion or proton is minor. The change in geometry is largest for the protonated systems and decreases with increasing size of the cation. Bond lengths and angles change in the most extreme cases by less than 0.06 Å and 7.0°, respectively. An interesting result is observed in the ortho-substituted complexes in that the metal ion is displaced toward the substituent, see Figure 4, and gains additional stabilization by interaction with the amino group. The displacement is metal ion dependent with ∠C4−N−$M^+$ angles of 151.3°, 155.5°, and 143.6° for the ortho-substituted complexes to $Li^+$, $Na^+$, and $K^+$, respectively. In contrast, the meta- and para-substituted complexes to all of the metals have ∠C4−N−M bond angles that are within 5.0° and 1.1° of linear, respectively. In the neutral *x*-$NH_2$Pyr molecules, the $NH_2$ group is nearly planar and almost $sp^2$-hybridized to allow delocalization of the lone pair electrons with the aromatic $\pi$-electrons of the pyridine ring. Upon metal ion complexation, chelation with the amino group requires that

**TABLE 2: Enthalpies and Free Energies of Metal Ion Binding to Aminopyridines at 298 K in kJ/mol[a]**

| system | $\Delta H_0$[b] | $\Delta H_0$[c] | $\Delta H_{298} - \Delta H_0$[c] | $\Delta H_{298}$ | $\Delta H_{298}$[c] | $T\Delta S_{298}$[c] | $\Delta G_{298}$ | $\Delta G_{298}$[c] |
|---|---|---|---|---|---|---|---|---|
| $H^+$(*o*-aminopyridine) | | 924.3 | 4.3 (1.7) | | 928.6 | 24.0 (3.1) | | 904.6 |
| $Li^+$(*o*-aminopyridine) | 237.8 (21.1) | 214.9 | 3.3 (1.7) | 241.1 (21.2) | 218.2 | 29.3 (4.3) | 211.8 (21.6) | 188.9 |
| $Na^+$(*o*-aminopyridine) | 146.5 (5.9) | 144.7 | 1.5 (1.3) | 148.0 (6.0) | 146.2 | 27.2 (4.2) | 120.8 (7.4) | 119.0 |
| $K^+$(*o*-aminopyridine) | 103.5 (3.6) | 103.9 | 1.1 (1.2) | 104.6 (3.8) | 105.0 | 28.4 (4.4) | 76.2 (5.8) | 76.6 |
| $H^+$(*m*-aminopyridine) | | 938.1 | 4.6 (1.5) | | 942.7 | 23.6 (3.2) | | 919.1 |
| $Li^+$(*m*-aminopyridine) | 201.7 (10.0) | 194.9 | 1.7 (1.6) | 203.4 (10.2) | 196.6 | 27.8 (4.0) | 175.6 (10.9) | 168.8 |
| $Na^+$(*m*-aminopyridine) | 136.1 (3.8) | 136.7 | 0.6 (1.3) | 136.7 (4.0) | 137.3 | 27.5 (4.4) | 109.2 (6.0) | 109.8 |
| $K^+$(*m*-aminopyridine) | 101.2(3.3) | 101.9 | 0.1 (1.0) | 101.3 (3.4) | 102.0 | 25.9 (4.8) | 75.4 (5.9) | 76.1 |
| $H^+$(*p*-aminopyridine) | | 958.5 | 5.7 (1.9) | | 964.2 | 25.9 (2.4) | | 938.3 |
| $Li^+$(*p*-aminopyridine) | 216.9 (20.2) | 208.4 | 0.5 (1.7) | 217.4 (20.3) | 208.9 | 24.5 (4.6) | 192.9 (20.8) | 184.4 |
| $Na^+$(*p*-aminopyridine) | 146.6 (4.6) | 146.5 | 0.2 (1.3) | 146.8 (4.8) | 146.7 | 27.1 (4.5) | 119.7 (6.6) | 119.6 |
| $K^+$(*p*-aminopyridine) | 108.9 (3.2) | 109.8 | 0.1 (1.0) | 108.8 (3.4) | 109.7 | 26.0 (4.8) | 82.8 (5.9) | 83.7 |

[a] Uncertainties are listed in parentheses. [b] Values taken from Table 1. [c] Ab initio values from calculations at the MP2(full)/6-311+G(2d,2p)//MP2(full)/6-31G* level of theory with frequencies scaled by 0.9646.

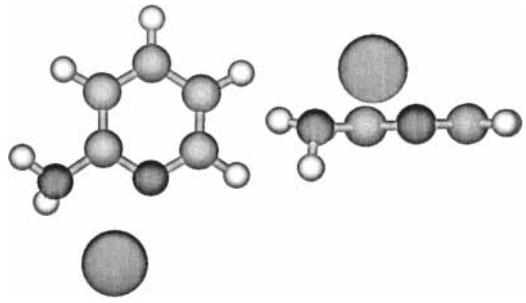

**Figure 5.** Optimized MP2(full)/6-31G* geometry of $K^+$(*o*-aminopyridine).

it rotate out of the plane of the molecule and rehybridize to $sp^3$. This rehybridization is indicated by the H−N−H bond angle, which changes from 112.4° in neutral *o*-$NH_2$Pyr to 105−106° in the metal complexes, and by the C2−$NH_2$ bond length, which increases by almost 0.06 Å upon metal complexation (Table S3). The $K^+$(*o*-$NH_2$Pyr) complex differs from all other complexes in that the $K^+$ does not lie in the plane of the molecule. The geometry is not that of a typical cation-$\pi$ complex in which the metal ion would be expected to lie roughly over the center of the aromatic $\pi$-system either. The preferred electrostatic binding interaction still involves a chelation interaction with the lone pairs of electrons on the pyridyl and amino N atoms. However, the rotation of the amino group out of the plane is less extensive to allow optimal interaction of the lone pair of electrons of the amino N atom with the $K^+$ ion; see Figure 5. There is too much steric hindrance to allow the $K^+$ ion to fit in the plane and interact strongly with the lone pair of electrons on the pyridyl and amino N atoms. However even in this distorted geometry, the binding is stronger than that to the $\pi$-cloud of the pyridine ring.

In the gas phase, we also need to consider the possibility of alternate tautomers to the structures shown in Figure 1, as such tautomers exist for both *o*-$NH_2$Pyr and *p*-$NH_2$Pyr and may be accessible in our gas-phase studies. However, in previous work on the interactions of alkali metal ions with azoles,[5] we demonstrated fairly conclusively that tautomerization of *N*-heterocycles in the gas phase or upon metal ion complexation did not occur. This was attributed to excessively high potential energy barriers between the possible complexes.[40] Rather, complexation to the most stable gas-phase tautomer of the free ligand was observed exclusively. For the *o*- and *p*-$NH_2$Pyr molecules, these are the tautomers identified in Figure 1. Our calculations indicate that the amino tautomers are more stable than the imino tautomers by 67.8 and 78.1 kJ/mol for *o*- and *p*-$NH_2$Pyr, respectively. In addition, the calculations find that the $Li^+$, $Na^+$, and $K^+$ complexes to the imino tautomers are less stable by 62.8, 60.4, and 60.1 kJ/mol, for the ortho-substituted complexes and 30.1, 40.0, and 47.2 kJ/mol, for the para-substituted complexes, respectively, than the analogous amino complexes (excluding ZPE and BSSE corrections). Thus, BDEs for $M^+$(*o*-iminopyridine) are 6.3, 7.9, and 8.6 kJ/mol and $M^+$(*p*-iminopyridine) are 42.5, 34.1, and 27.6 kJ/mol, respectively, stronger than those of the ground-state $M^+$(*x*-$NH_2$Pyr) complexes. This assumes that tautomerization does not occur upon CID, an assumption consistent with the results of our previous studies.[5] If tautomerization could occur upon formation of the complexes (i.e., the barrier to tautomerization is lower than the BDE to the amino tautomer), then the reverse process, tautomerization upon CID, would also occur. This would lead to much weaker bond dissociation energies, 152.1, 84.3, and 43.8 kJ/mol for the $Li^+$, $Na^+$, and $K^+$ complexes, respectively.

**Conversion from 0 to 298 K.** To allow comparison to commonly used experimental conditions, we convert the 0 K bond energies determined here (experimentally and theoretically) to 298 K bond enthalpies and free energies. The enthalpy and entropy conversions are calculated using standard formulas (assuming harmonic oscillator and rigid rotor models) and the vibrational and rotational constants determined for the MP2(full)/6-31G* optimized geometries, which are given in Tables S1 and S2. Table 2 lists 0 and 298 K enthalpy, free energy, and enthalpic and entropic corrections for all systems experimentally determined (from Table 1). Uncertainties in the enthalpic and entropic corrections are determined by 10% variation in the molecular constants. For the metal systems where the metal−ligand frequencies are very low and may not be adequately described by theory, the listed uncertainties also include changing the three metal−ligand frequencies by a factor of 2. The latter provides a conservative estimate of the computational errors in these low-frequency modes and is the dominant source of the uncertainties listed.

## Discussion

**Comparison of Theory and Experiment.** The metal cation affinities of the three structural isomers of *x*-$NH_2$Pyr at 0 K measured here by guided ion beam mass spectrometry are summarized in Table 3. Also listed here are the 0 K proton and metal binding energies calculated at the MP2(full)/6-311+G(2d,2p)//MP2(full)/6-31G* level including full MP2 correlation, zero point energy corrections, and basis set superposition error corrections.[41−43] Experimental and theoretical results for the unsubstituted pyridine molecule taken from previous studies are also provided in Table 3 for comparison.[8,44−46] The agreement between theory and experiment is illustrated in Figure 6. It can be seen that the agreement is very good over the nearly 140 kJ/mol variation in binding affinities measure here. For the nine

**TABLE 3: Measured and Calculated Enthalpies of Proton and Alkali Metal Ion Binding to Aminopyridines at 0 K in kJ/mol**

| | experiment X=$NH_2$ | | theory X=$NH_2$ (MP2) | | | experiment X=Me[a] |
|---|---|---|---|---|---|---|
| complex | TCID[b] | literature | $D_e$[c] | $D_0$[d] | $D_{0,BSSE}$[e] | TCID |
| $H^+$(*o*-Xpyridine) | | 942.9 (16.0)[f] | 966.4 | 934.0 | 924.3 | |
| $Li^+$(*o*-Xpyridine) | 237.8 (21.1) | | 231.3 | 222.8 | 214.9 | 194.3 (6.5) |
| $Na^+$(*o*-Xpyridine) | 146.5 (5.9) | | 158.4 | 153.4 | 144.7 | 128.2 (4.5) |
| $K^+$(*o*-Xpyridine) | 103.5 (3.6) | | 112.8 | 108.6 | 103.9 | 97.8 (3.3) |
| $H^+$(*m*-Xpyridine) | | 949.8 (16.0)[f] | 981.2 | 947.6 | 938.1 | |
| $Li^+$(*m*-Xpyridine) | 201.7 (10.0) | | 205.5 | 200.7 | 194.9 | 196.6 (14.7) |
| $Na^+$(*m*-Xpyridine) | 136.1 (3.8) | | 145.8 | 143.1 | 136.7 | 133.3 (4.2) |
| $K^+$(*m*-Xpyridine) | 101.2 (3.3) | | 107.5 | 105.7 | 101.9 | 99.8 (3.3) |
| $H^+$(*p*-Xpyridine) | | 974.0 (16.0)[f] | 1003.3 | 968.0 | 958.5 | |
| $Li^+$(*p*-Xpyridine) | 216.9 (20.2) | | 217.8 | 214.2 | 208.4 | 196.2 (13.4) |
| $Na^+$(*p*-Xpyridine) | 146.6 (4.6) | | 155.2 | 153.0 | 146.5 | 133.7 (3.8) |
| $K^+$(*p*-Xpyridine) | 108.9 (3.2) | | 115.1 | 113.5 | 109.8 | 98.8 (3.9) |
| $H^+$(pyridine) | | 924.0 (16.0)[f] | 954.8[g] | 918.4[g] | 908.9[g] | |
| $Li^+$(pyridine) | 181.0 (14.5)[g] | 181.2 (9.5)[h] | 190.7[g] | 185.7[g] | 179.1[g] | |
| $Na^+$(pyridine) | 126.7 (2.9)[g] | | 133.6[g] | 130.1[g] | 122.9[g] | |
| $K^+$(pyridine) | 90.3 (3.9)[g] | | 97.2[g] | 94.6[g] | 91.1[g] | |

[a] See Rodgers.[11] [b] Present results, threshold collision-induced dissociation. [c] Calculated at the MP2(full)/6-311+G(2d,2p) level of theory using MP2(full)/6-31G* optimized geometries. [d] Including zero point energy corrections with frequencies scaled by 0.9646. [e] Also includes basis set superposition error corrections. [f] See Hunter and Lias.[47] Adjusted to 0 K. [g] See Amunugama and Rodgers.[8] [h] See earlier works.[44−46] Adjusted to 0 K.

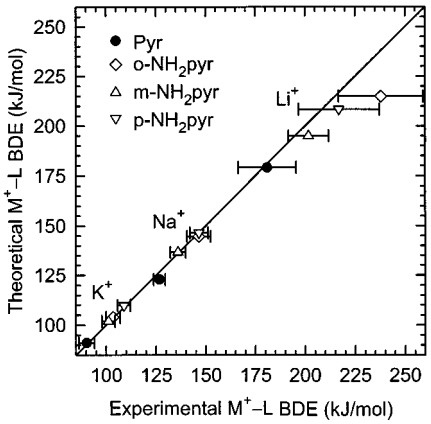


**Figure 6.** Theoretical versus experimental bond dissociation energies (in kJ/mol) of $M^+$−(*x*-aminopyridine), where $M^+ = Li^+$, $Na^+$, and $K^+$, and *x* = ortho (◇), meta (△), and para (▽). All values are at 0 K and taken from Table 3. Experimental results include values for the unsubstituted pyridine systems, taken from a previous study[8] (●). The diagonal line indicates the values for which calculated and measured bond dissociation energies are equal.

amino-substituted systems, the mean absolute deviation (MAD) between experiment and theory is 5.6 ± 8.2 kJ/mol. This is slightly smaller than the average experimental error of 8.4 ± 7.3 kJ/mol. However, more careful inspection of the data makes it clear that $Li^+$ is the principal contributor to the deviations. For the three $Li^+$ systems, the MAD is 15.4 ± 7.2 kJ/mol, whereas the $Na^+$ and $K^+$ systems have a MAD of 0.8 ± 0.6 kJ/mol. The poorer agreement for the $Li^+$ systems most likely results from the experimental difficulty in measuring cross sections for $Li^+$ as a result of the difficulty associated with efficient detection of this light mass as discussed in the Experimental Section. An alternative explanation was proposed in an earlier study[9] where it was also observed that theory systematically underestimates the bond energies for the $Li^+$ complexes, which may be a result of the higher degree of covalency in the metal−ligand bond (see discussion below). The additional covalency of the metal−ligand bonds in the $Li^+$ systems compared to those for $Na^+$ and $K^+$ suggests that this level of theory may be inadequate for a complete description of the former systems. Some evidence for this is the large discrepancy between theoretical and experimental values for the protonated systems,[47] Table 3, which are clearly covalent. The MAD for the three protonated systems is 15.3 ± 3.5 kJ/mol. However, it is also possible that this additional covalency means that the TSs for dissociation of the $Li^+$ complexes are not adequately described by the PSL model. If the transition states were tighter in the $Li^+$ cases, then the kinetic shifts would be larger and the thresholds measured smaller, in better agreement with theory. For the $Na^+$ and $K^+$ complexes, the kinetic shifts are much smaller and the metal−ligand bonds more electrostatic, such that the treatment here is most assuredly appropriate and would not change greatly with different assumptions about the TS.

As discussed above, the imino tautomers are not expected to play a role in these systems based upon their relative stability compared to the amino tautomers. The theoretical BDEs used in the comparison between theory and experiment in Table 3 and Figure 6 are for the amino tautomers. The good agreement between theory and experiment supports the assumption that the imino tautomers do not play a role in these systems. The large difference in BDEs for the para-substituted complexes to the amino and imino tautomers absolutely rule out the possibility that the imino tautomers play a role in the para-substituted systems. However, the small difference in the BDEs for the ortho-substituted complexes to these two tautomers makes it difficult to establish definitively which tautomer is present in the ortho-substituted complexes by comparison to the experimental values. In addition, the barrier to tautomerization in the ortho-substituted complexes is expected to be significantly lower than for the para-substituted systems as a result of the proximity of the H atom to the two binding sites. However, the complexes are formed by association of the gas-phase neutral with the metal ion in the flow tube, such that either tautomerization does not occur upon association/CID or, if it does, then the measured BDEs do not agree with theory as discussed above. Therefore, the imino tautomer cannot play a role in the ortho systems.

**Trends in the Binding of Metal Ions to *x*-Aminopyridines.** In all of the *x*-$NH_2$Pyr systems, the binding strength varies with the metal ion such that $Li^+$ binds ∼53% more strongly than $Na^+$, which in turn binds ∼37% more strongly than $K^+$. Because these complexes are largely electrostatic in nature, this trend is easily understood on the basis of the size, or equivalently, the

charge density of the metal ion. Smaller metal ions lead to stronger ion−dipole and ion-induced dipole interactions in these systems because the metal−ligand bond distances are smaller. In this simplistic point of view, the strength of the interaction of the metal ions with the *x*-aminopyridines appears to be driven principally by the ion-induced dipole interaction, which does not change appreciably for these structurally similar ligands.

Theoretical calculations indicate that the charge retained on the metal ions is fairly similar from one structural isomer to another: $Li^+$ has a charge of ~0.76*e*, which is lower than that for $Na^+$ (~0.92*e*), which is lower than that for $K^+$ (~0.98*e*). These results confirm the electrostatic nature of the bonding, but also demonstrate that there is some covalency in the metal−ligand interaction, particularly in the $Li^+$ systems. In these complexes, the shorter bond distance and greater charge density allow the metal ion to more effectively withdraw electron density from the neutral ligand, thus reducing the charge retained on the metal ion and increasing the covalency of the metal−ligand interaction.

The primary effect that the amino substituent has upon the binding can be examined by comparing these systems to the unsubstituted pyridine molecule. The polarizability of pyridine is estimated to be 9.51 Å$^3$ and increases to 10.63 Å$^3$ upon amino substitution.[13] The polarizability is not expected to vary significantly with the position of the amino substituent, and the additivity method we used to estimate these polarizabilities is not sensitive to such structural differences. The binding affinity of all nine complexes is observed to increase upon amino substitution relative to that observed for the corresponding pyridine complexes; see Table 3 and Figure 6. This suggests that the polarizability of the ligand is a key factor in determining the strength of binding.

Smaller variations in the strength of the binding are observed as the position of the substituent is varied. These variations can be attributed to several possible effects: the dipole moment of the molecule, inductive effects, resonance effects, chelation interaction, and steric effects. As seen in Figure 1, the dipole moment of these systems follows the order ortho (2.05 D) < meta (3.12 D) < para (3.69 D). The calculated dipole moment of pyridine is 2.22 D, implying that if the dipole moment plays a more important role than the polarizability in determining the binding strength, that the ortho-substituted complexes should have lower binding affinities than pyridine. This is not the case, Table 3, suggesting that the polarizability is more important than the dipole moment of the ligand in determining the strength of binding as mentioned above. The dipole moment may still play a role, albeit less significant, and suggests that the binding affinities should follow the order ortho < meta < para. Indeed, this is the order observed in the protonated complexes, where the longer-range electrostatic interactions are not expected to play as strong a role as for the metalated systems. However, this trend is not observed for the metalated systems, indicating that other effects unique to the metal ions are operative. Because of the electron-withdrawing properties of the amino substituent, inductive effects suggest that the binding affinities should follow the order para < meta < ortho, again the order observed for the protonated complexes. However, this order is not observed for the metalated complexes, Table 3, suggesting that inductive effects are not significant. In the ortho- and para-substituted complexes, contributions from resonance structures that localize electron density on the pyridyl nitrogen atom (as shown below) should result in enhanced binding compared to the analogous meta complexes and suggest that the binding affinities should follow the order meta < ortho ≈ para.

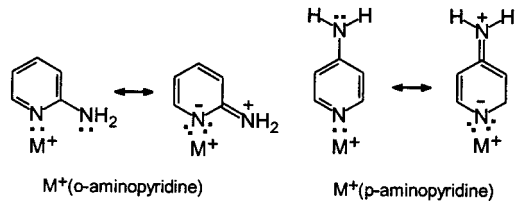


In all cases, the meta systems are less strongly bound than the corresponding ortho- and para-substituted systems, confirming that resonance effects do play an important role in determining the strength in the binding of these systems. However, the strength of the binding in the ortho- and para-substituted systems changes with the metal ion, suggesting that additional effects are operative. Both theory and experiment find that the relative binding affinities are metal ion dependent and follow the order meta < para < ortho for $Li^+$, meta < ortho ≈ para for $Na^+$, and meta < ortho < para for $K^+$, Table 3. The metal ion dependence of the relative binding to the ortho- and para-substituted systems is a balance between three competing effects, all associated with the interaction of the metal ion with the amino group in the ortho-substituted systems. In all three ortho-substituted complexes, the amino group rotates out of the plane, and the metal ion orients itself such that it is actually tilted toward the amino substituent by 28.7°, 24.5°, and 36.7° for the $Li^+$, $Na^+$ and $K^+$ systems, respectively (Figure 4). The ability of the metal ion to chelate effectively with the amino group is the driving force for this tilt and suggests there is a significant chelation (attractive interaction) with the adjacent amino group rather than a steric effect (repulsive interaction). Thus, $Na^+$ tilts 4.2° less toward the amino group than $Li^+$ because of the longer $M^+$−N bond distances. The angle in the $K^+$ complex is somewhat deceiving in that the $K^+$ ion lies out of the plane of the molecule, Figure 5. Rotation of the amino group out of the plane (i) decreases stabilization associated with $\pi$-resonance delocalization, (ii) decreases repulsion between the metal ion and nearest H atom when the amino group is planar, and (iii) enhances binding as a result of chelation. The combination of these effects leads to chelation for all three metal ions, as indicated by theory, which finds that the most stable conformations of the $M^+$(*o*-$NH_2$Pyr) complexes have the amino group rotated out of the plane.

The first effect, $\pi$-resonance delocalization, should in principle have little dependence upon the metal ion. This effect is estimated as the difference in energies of the free *o*-$NH_2$Pyr in its most stable conformation and that of free *o*-$NH_2$Pyr in the distorted geometries of the $M^+$(*o*-$NH_2$Pyr) complexes. These calculations indicate that the distortion cost is about the same for $Li^+$ and $Na^+$, (46.3 and 43.6 kJ/mol, respectively), but only costs 24.9 kJ/mol for the $K^+$. The lower cost in the $K^+$ system results from the lesser degree of rotation of the amino group in the $K^+$(*o*-$NH_2$Pyr) complex. We estimate the second effect, H-atom repulsion, by calculating the binding energies of the three metal ions at the pyridyl N atom site of *o*-$NH_2$Pyr with its geometry fixed to that of the free *o*-$NH_2$Pyr, i.e., roughly planar. These complexes are less stable than the fully optimized complexes by 53.4, 35.7, and 16.6 kJ/mol for $Li^+$, $Na^+$, and $K^+$, respectively. We take these values to be a rough estimate of the H-atom repulsive energy. Combining the results of these calculations with the measured BDEs to *o*- and *p*-$NH_2$Pyr (Table 3), we arrive at estimates for the chelation effect, which is strongest for $Li^+$, 121 kJ/mol, and decreases for the larger metal ions, ~79 kJ/mol for $Na^+$ and ~36 kJ/mol for $K^+$. Thus, $Li^+$ binds *o*-$NH_2$Pyr more strongly than *p*-$NH_2$Pyr because the chelation energy is larger than the sum of the $\pi$-resonance

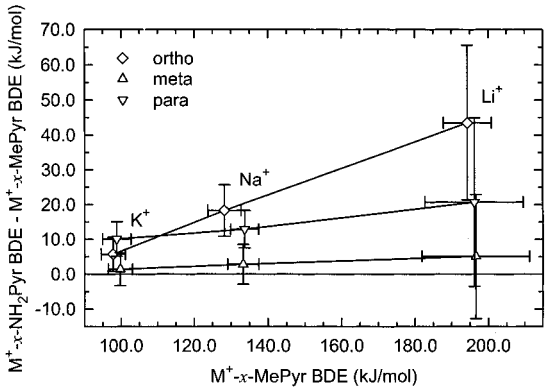


**Figure 7.** Measured difference in the bond dissociation energies of $M^+-$(*x*-aminopyridine) relative to $M^+-$(*x*-methylpyridine) versus the bond dissociation energies of $M^+-$(*x*-methylpyridine), where $M^+ = Li^+$, $Na^+$, and $K^+$, and $x$ = ortho (◇), meta (△), and para (▽). All values are at 0 K and taken from Table 3 and a previous study.[11] The horizontal line indicates the values for which no difference in the binding is observed.

delocalization energy lost and the H-atom repulsion energy. For $Na^+$, the H-atom repulsion energy increases and the chelation energy decreases such that these contributions balance. Although the resonance delocalization energy decreases for $K^+$, the H-atom repulsion energy becomes great enough that the complex is not able to exist in a geometry that is ideally suited to maximizing the chelation interaction, and the metal ion sits out of the plane. As a result of taking on a less favorable geometry, the sum of these two effects (resonance delocalization energy loss and H-atom repulsion) is larger than the chelation energy, resulting in weaker binding to *o*- than to *p*-$NH_2$Pyr.

Both theory and experiment find that the meta systems bind more weakly than the para-substituted systems, in agreement with the expected order based upon the dipole moments of these molecules and resonance effects. But, it has already been established in the ortho-substituted systems that the chelation interaction has a greater influence on the binding than inductive effects of the substituent. This suggests that the influence of the dipole moment and inductive effects on the binding to these systems is quite small. Overall, the observed trends in the binding of alkali metal ions to these systems are therefore dominated by the charge density of the metal ion, and secondarily by the polarizability of the ligand. As these effects are the same for all three structural isomers, the modest variations in binding affinity observed result from chelation interactions with some contributions from resonance effects. The dipole moment of the ligand and inductive effects appear to have only a small influence on the binding in these systems.

**Comparison with the *x*-Methylpyridines.** Figure 7 compares the present experimental results to those obtained in an earlier study from our laboratory in which the binding of the same alkali metal ions to the *x*-methylpyridines (*x*-MePyr) was examined. The most obvious conclusion that can be drawn from this figure is the *x*-$NH_2$Pyr systems are more strongly bound than the corresponding *x*-MePyr systems. This seems counter-intuitive based upon the polarizabilities of these systems (10.63 $Å^3$ for *x*-$NH_2$Pyr vs 11.35 $Å^3$ for *x*-MePyr) and allows further examination of the influence that the dipole moment and resonance effects have upon the binding in these systems. Because resonance effects do not enhance binding in the meta systems, the increased binding affinities measured for $M^+$(*m*-$NH_2$Pyr) compared to $M^+$(*m*-MePyr) suggest that the larger dipole moment of *m*-$NH_2$Pyr (3.12 D) vs *m*-MePyr (2.62 D) is more than sufficient to overcome the decrease in polarizability. As expected, the effect is metal ion dependent and results in an increase in binding affinity of 5, 3, and 1 kJ/mol for the $Li^+$, $Na^+$, and $K^+$ systems, respectively. However, the influence of the dipole moment is small compared to the increase in binding affinity observed in the ortho- and para-substituted systems where resonance effects and chelation interactions lead to stronger binding. In the para-substituted systems, the increase in dipole moment is larger than that for the meta systems, *p*-$NH_2$-Pyr (3.69 D) vs *p*-MePyr (2.89 D). Assuming an approximately linear correlation between the binding affinity and the increase in the dipole moment ($NH_2$ vs Me), the dipole moment contribution to the enhancement in the binding affinities of *p*-$NH_2$Pyr compared to *p*-MePyr would be 8, 4, and 2 kJ/mol for the $Li^+$, $Na^+$, and $K^+$ systems, respectively. The observed enhancement in the BDEs to *p*-$NH_2$Pyr compared to those measured for *p*-MePyr is much larger than the contribution predicted from the enhanced dipole moment of *p*-$NH_2$Pyr. This suggests that the contribution to the binding affinity resulting from resonance effects is >60% of the enhancement. The resonance effects contribution is estimated to be 13, 8, and 8 kJ/mol for the $Li^+$, $Na^+$, and $K^+$ systems, respectively. In the ortho-substituted systems, the increase in dipole moment is much smaller than that for the meta-substituted systems, *o*-$NH_2$Pyr (2.05 D) vs *o*-MePyr (1.97 D), and likely balances the decrease in polarizability. This suggests that the difference in binding affinities for the ortho systems results from resonance effects and the much stronger chelation interaction possible in the *o*-$NH_2$Pyr systems. The alternate possibility of repulsive steric interactions in the *o*-MePyr systems was previously shown to be unimportant and in fact that the methyl substituent exhibits a slight chelation interaction.[11] As the influence of dipole moment on the binding was not taken into consideration in the estimation of the chelation effect above, the influence of the chelation effect was probably underestimated. Thus a better estimation of the chelation effect in the *o*-$NH_2$Pyr systems would be obtained by correcting for the differences in dipole moment of the *o*- and *p*-$NH_2$Pyr systems (as the resonance effects cancel). The relative enhancement in dipole moment compared to the meta isomers should result in an enhancement in binding of the *p*-$NH_2$Pyr compared to the analogous *o*-$NH_2$Pyr systems of 7, 4, and 2 kJ/mol for the $Li^+$, $Na^+$, and $K^+$ systems, respectively. Thus, the chelation effect enhances binding in the *o*-$NH_2$Pyr systems by 128, 83, and 38 for the $Li^+$, $Na^+$, and $K^+$ systems, respectively.

## Conclusions

The kinetic energy dependences of the collision-induced dissociation of $M^+$(*x*-$NH_2$Pyr), where $M^+ = Li^+$, $Na^+$, and $K^+$, and $x$ = ortho, meta, and para with Xe are examined in a guided ion beam mass spectrometer. The dominant dissociation process in all cases is loss of the intact *x*-$NH_2$Pyr ligand. Thresholds for these processes are determined after consideration of the effects of reactant internal energy, multiple collisions with Xe, and lifetime effects (using methodology described in detail elsewhere).[3] Insight into the structures and binding of the metal ions to the *x*-$NH_2$Pyr molecules is provided by ab initio theory calculations of these complexes performed at the MP2(full)/6-311+G(2d,2p)//MP2(full)/6-31G* level of theory. Excellent agreement between the experimentally determined $Na^+$ and $K^+$ affinities and ab initio calculations is obtained. Although within experimental error, the agreement for the $Li^+$ systems is not quite as good. Several plausible explanations for this discrepancy are proposed. The high fidelity of our experimental and theoretical results suggests that these ligands can act as reliable

anchors for the alkali metal cation affinity scales. These systems broaden the range of ligands available as absolute thermochemical anchors. Further, the combined theoretical and experimental results suggest that the strength of the noncovalent interaction of alkali metal ions with the *x*-aminopyridines is dominated by the charge density of the metal ion. The polarizability of the ligand is also an important factor in determining the strength of the binding. As these effects are the same for all three structural isomers, the pronounced variations in binding affinity observed result from chelation interactions with some contributions from resonance effects. The dipole moment of the ligand and inductive effects also appear to influence the binding in these systems but to a lesser degree. The differences in the trends in the BDEs observed for the *x*-$NH_2$Pyr systems compared to the *x*-$CH_3$Pyr systems can be understood in terms of the differences in polarizability, dipole moment of these systems and the contributions from resonance effects possible only in the *x*-$NH_2$Pyr systems.

**Acknowledgment.** This work was supported in part by an ASMS Research Award from Micromass.

**Supporting Information Available:** Tables of vibrational frequencies, average vibrational energies, rotational constants, and MP2(full)/6-31G(d) geometry optimized structures for neutral, protonated, and metalated *x*-aminopyridines. Figures showing cross sections for the collision-induced dissociation of $M^+$(*x*-aminopyridines) complexes as well as empirical fits to the $M^+$ product channels (PDF). This material is available free of charge via the Internet at http://pubs/acs/org.

## References and Notes

(1) Rodgers, M. T.; Armentrout, P. B. *J. Phys. Chem. A* **1997**, *101*, 1238.
(2) Rodgers, M. T.; Armentrout, P. B. *J. Phys. Chem. A* **1997**, *101*, 2614.
(3) Rodgers, M. T.; Ervin, K. M.; Armentrout, P. B. *J. Chem. Phys*. **1997**, *106*, 4499.
(4) Rodgers, M. T.; Armentrout, P. B. *J. Chem. Phys.* **1998**, *109*, 1787.
(5) Rodgers, M. T.; Armentrout, P. B. *Int. J. Mass Spectrom*. **1999**, *185*−*187*, 359.
(6) Rodgers, M. T.; Armentrout, P. B. *J. Phys. Chem. A* **1999**, *103*, 4955.
(7) Armentrout, P. B.; Rodgers, M. T. *J. Phys. Chem. A* **2000**, *104*, 2238.
(8) Amunugama, R.; Rodgers, M. T. *Int. J. Mass Spectrom*. **2000**, *195*/*196*, 439.
(9) Rodgers, M. T.; Armentrout, P. B. *J. Am. Chem. Soc.* **2000**, *122*, 8548.
(10) Rodgers, M. T.; Stanley, J. R.; Amunugama, R. *J. Am. Chem. Soc*. **2000**, *122*, 10969.
(11) Rodgers, M. T. *J. Phys. Chem. A* **2001**, *105*, 2374.
(12) Amunugama, R.; Rodgers, M. T. *J. Phys. Chem. A*, submitted for publication.
(13) Miller, K. J. *J. Am. Chem. Soc*. **1990**, *112*, 8533.
(14) Teloy, E.; Gerlich, D. *Chem. Phys.* **1974**, *4*, 417. Gerlich, D. Diplomarbeit, University of Freiburg, Federal Republic of Germany, 1971. Gerlich, D. In *State-Selected and State-to-State Ion*−*Molecule Reaction Dynamics: Part 1, Experiment*; Ng, C.-Y., Baer, M., Eds.; Adv. Chem. Phys. **1992**, *82*, 1.
(15) Dalleska, N. F.; Honma, K.; Armentrout, P. B. *J. Am. Chem. Soc.* **1993**, *115*, 12125.
(16) Aristov, N.; Armentrout, P. B. *J. Phys. Chem.* **1986**, *90*, 5135.
(17) Hales, D. A.; Armentrout, P. B. *J. Cluster Sci.* **1990**, *1*, 127.
(18) Ervin, K. M.; Armentrout, P. B. *J. Chem. Phys*. **1985**, *83*, 166.
(19) Dalleska, N. F.; Honma, K.; Sunderlin, L. S.; Armentrout, P. B. *J. Am. Chem. Soc.* **1994**, *116*, 3519.
(20) Schultz, R. H.; Armentrout, P. B. *J. Chem. Phys*. **1992**, *96*, 1046.
(21) Schultz, R. H.; Crellin, K. C.; Armentrout, P. B. *J. Am. Chem. Soc.* **1992**, *113*, 8590.
(22) Khan, F. A.; Clemmer, D. C.; Schultz, R. H.; Armentrout, P. B. *J. Phys. Chem*. **1993**, *97*, 7978.
(23) Fisher, E. R.; Kickel, B. L.; Armentrout, P. B. *J. Phys. Chem.* **1993**, *97*, 10204.
(24) Frisch, M. J.; Trucks, G. W.; Schlegel, H. B.; Scuseria, G. E.; Robb, M. A.; Cheeseman, J. R.; Zakrzewski, V. G.; Montgomery J. A., Jr.; Stratmann, R. E.; Burant, J. C.; Dapprich, S.; Millam, J. M.; Daniels, A. D.; Kudin, K. N.; Strain, M. C.; Farkas, O.; Tomasi, J.; Barone, V.; Cossi, M.; Cammi, R.; Mennucci, B.; Pomelli, C.; Adamo, C.; Clifford, S.; Ochterski, J.; Petersson, G. A.; Ayala, P. Y.; Cui, Q.; Morokuma, K.; Malick, D. K.; Rabuck, A. D.; Raghavachari, K.; Foresman, J. B.; Cioslowski, J.; Ortiz, J. V.; Stefanov, B. B.; Liu, G.; Liashenko, A.; Piskorz, P.; Komaromi, I.; Gomperts, R.; Martin, R. L.; Fox, D. J.; Keith, T.; Al-Laham, M. A.; Peng, C. Y.; Nanayakkara, A.; Gonzalez, C. Challacombe, M.; Gill, P. M. W.; Johnson, B.; Chen, W. Wong, M. W.; Andres, J. L.; Gonzales, C.; Head-Gordon, M.; Replogle, E. S.; Pople, J. A. *Gaussian 98*, rev. A.7; Gaussian, Inc.: Pittsburgh, PA, 1998.
(25) Foresman, J. B.; Frisch, Æ. *Exploring Chemistry with Electronic Structure Methods*, 2nd ed.; Gaussian: Pittsburgh, 1996.
(26) Beyer, T. S.; Swinehart, D. F. *Comm. Assoc. Comput. Machines* **1973**, *16*, 379. Stein, S. E.; Rabinovitch, B. S. *J. Chem. Phys*. **1973**, *58*, 2438; *Chem. Phys. Lett*. **1977**, *49*, 1883.
(27) Pople, J. A.; Schlegel, H. B.; Raghavachari, K.; DeFrees, D. J.; Binkley, J. F.; Frisch, M. J.; Whitesides, R. F.; Hout, R. F.; Hehre, W. J. *Int. J. Quantum Chem. Symp*. **1981**, *15* 269. DeFrees, D. J.; McLean, A. D. *J. Chem. Phys.* **1985**, *82*, 333.
(28) Waage, E. V.; Rabinovitch, B. S. *Chem. Rev.* **1970**, *70*, 377.
(29) Chesnavich, W. J.; Bowers, M. T. *J. Phys. Chem.* **1979**, *83*, 900.
(30) Armentrout, P. B., In *Advances in Gas-Phase Ion Chemistry*; Adams, N. G., Babcock, L. M., Eds.; JAI: Greenwich, 1992; Vol. 1, pp 83−119.
(31) See, for example: Sunderlin, L. S.; Armentrout, P. B. *Int. J. Mass Spectrom. Ion Processes* **1989**, *94*, 149.
(32) More, M. B.; Glendening, E. D.; Ray, D.; Feller, D.; Armentrout, P. B. *J. Phys. Chem.* **1996**, *100*, 1605.
(33) Ray, D.; Feller, D.; More, M. B.; Glendening, E. D.; Armentrout, P. B. *J. Phys. Chem.* **1996**, *100*, 16116.
(34) Meyer, F.; Khan, F. A.; Armentrout, P. B. *J. Am. Chem. Soc.* **1995**, *117*, 9740.
(35) See, for example, Figure 1.[15]
(36) Armentrout, P. B.; Simons, J. *J. Am. Chem. Soc.* **1992**, *114*, 8627.
(37) Meyer, F.; Khan, F. A.; Armentrout, P. B. *J. Am. Chem. Soc*. **1995**, *117*, 9740.
(38) Lifshitz, C. *Adv. Mass Spectrom*. **1989**, *11*, 113.
(39) Figures were generated using the output of *Gaussian98* geometry optimizations in Hyperchem Computational Chemistry Software Package, Ver. 5.0, Hypercube Inc., 1997.
(40) Wong, M. W.; Leung-Toung, R.; Wentrup, C. *J. Am. Chem. Soc.* **1993**, *115*, 2465 and references therein.
(41) Møller, C.; Plesset, M. S. *Phys. Rev.* **1934**, *46*, 618.
(42) Bartlett, R. J. *Annu. Rev. Phys. Chem.* **1981**, *32*, 359.
(43) Hehre, W. J.; Radom, L.; Schleyer, P. v. R.; Pople, J. A. *Ab Initio Molecular Orbital Theory*; Wiley: New York, 1986.
(44) Anvia, F.; Walsh, S.; Capon, M.; Koppel, I. A.; Taft, R. W.; de Paz, J. L. G.; Catalan, J. *J. Am. Chem. Soc.* **1990**, *112*, 5095.
(45) Taft, R. W.; Anvia, F.; Gal, J.-F.; Walsh, S.; Capon, M.; Holmes, M. C.; Hosn, K.; Oloumi, G.; Vasanwala, R.; Yazdani, S. *Pure Appl. Chem.* **1990**, *62*, 17.
(46) Burk, P.; Koppel, I. A.; Koppel, I.; Kurg, R.; Gal, J.-F.; Maria, P.-C.; Herreros, M.; Notario, R.; Abboud, J.-L. M.; Anvia, F.; Taft, R. W. *J. Phys. Chem. A* **2000**, *104*, 2824.
(47) Hunter, E. P.; Lias, S. G. Proton Affinity Evaluation in NIST Chemistry WebBook. *NIST Standard Reference Database*, no. 69; Mallard, W. G.; Lindstrom, P. J., Eds.; National Institute of Standards and Technology: Gaithersburg, MD, 1998; accessible at http://webbook.nist.gov.